Article | Received 26 May 2023; Accepted 25 June 2023; Published 12 July 2023
https://doi.org/10.55092/bm20230005

The effect of high salinity on the infectivity of H1N1 and SARS-CoV-2 viruses

Kuan-Che Feng[1,*,†], Jacob F. Myers[1,2,†], Kaitlyn Swayze[3,†], Fan Yang[1], Won-Il Lee[1], Steffen Mueller[4], Ashhad Khan[5], Karin Hasegawa[5], Marcia Simon[6], Kalle Levon[7], Peng Zhang[5], Yuefan Deng[5,*] Miriam Rafailovich[1]

[1] Department of Materials Science and Chemical Engineering, Stony Brook University, Stony Brook, 11794, USA
[2] Department of Microbiology and Immunology, Sidney Kimmel Medical College, Philadelphia, 19107, USA
[3] Department of Biomedical Engineering, Stony Brook, Stony Brook University, 11794, USA
[4] Codagenix Inc., Farmingdale, 11735, USA
[5] Department of Applied Mathematics and Statistics, Stony Brook University, Stony Brook, 11794, USA
[6] Department of Oral Biology and Pathology, Stony Brook University, Stony Brook, 11794, USA
[7] Department of Chemical and Biomolecular Engineering, New York University, Brooklyn, 11201, USA

* Corresponding authors; E-mails: kuanche.feng@gmail.com, yuefan.deng@stonybrook.edu.

† K-C.F., J.F.M. and K.S. contributed equally to this paper.

Abstract: Viral particles are transmitted via air-borne respiratory droplets containing salt, surfactants and other solutes. The drying dynamics of droplets increase internal saline concentrations, impacting viral viability. Plaque assays were used to quantify the infectivity of H1N1 and SARS-CoV-2 viruses after being placed in NaCl solutions of different concentrations at ambient conditions. Changes in structure of the SARS-CoV-2 spike protein after immersion in NaCl solutions were measured using the 3D molecular imprinting technique. In silico simulation of the S-protein structure in contact with different concentrations of NaCl were performed using GROMACS 2020.2 on the AiMOS supercomputer built with IBM POWER9. Plaque assays showed that both H1N1 and SARS-CoV-2 virus infectivity were changed by less than one log reduction after treatment with high salt solutions up to 5M. No change in structure was detected with the 3D molecular imprinted sensors even at the highest concentration. The results were confirmed using molecular dynamics simulations. We have found that incubation in NaCl solutions, up to 5M concentration, had only a minimal affect in reducing the infectivity of H1N1 and SARS-CoV-2 viruses. In silico modeling and molecular imprinting measurements of the S-proteins indicated no change in molecular structure, consistent with maintaining

infectivity. Hence in contrast to their anti-bacterial efficacy, high salt solutions are ineffective as an anti-viral agent.

Keywords: SARS-CoV-2; H1N1 influenzas virus; salinity; 3D molecular imprinted sensors; in silico simulation; S-protein; molecular dynamics simulations

1. Introduction

Since emerging in late 2019, SARS-CoV-2 has caused well over seven million documented deaths and nearly unprecedented levels of social and economic disruption[1]. As the world begins to coexist with SARS-CoV-2, we must consider threats the future might hold.

While SARS-CoV-2 was and remains a devastating public health issue, a lack of surface transmission[2–4] did mean that many daily activities remained safe throughout the pandemic. Early on, several studies were published detailing superspreader events associated with respiratory droplets in contexts like choirs[5], concerts[6], and workplaces[7], but not associated with fomites, like package delivery. To date, there remain very few published examples of patients falling ill with SARS-CoV-2 from fomites, and in these cases, respiratory droplet contacts can rarely be ruled out[4,8]. Though, it is worth noting that transmission occurring on very high-traffic surfaces, like door handles in public spaces, would necessarily be confounded by exposure to respiratory droplets. A lack of surface transmission is different from what might be expected based on numerous studies which found SARS-CoV-2 able to remain infectious on surfaces for extended periods[9–12].

SARS-CoV-2 is only the most recent respiratory virus to threaten public health. Influenza is estimated to cause hundreds of thousands of deaths every year[13] and, similar to SARS-CoV-2, is thought to be spread primarily by respiratory droplets[14]. Like SARS-CoV-2, Influenza has also been shown to survive on fomites for long periods of time[15–18], but unlike SARS-CoV-2, there is compelling data supporting fomites contributing to human Influenza infections[19,20].

Respiratory droplets vary in size greatly, from aerosols that can remain suspended in the air, to the large droplets responsible for SARS-CoV-2 and Influenza transmission[2,14] which generally settle quickly due to gravity[21]. The size differentiating these two categories of droplets is generally thought to be around 10 μm in diameter, or 500 fL[22], though large droplets can be upwards of 2 uL[23]. Infection requires that susceptible tissues in the host be exposed to a given number of virions. Hence airborne droplets are more efficient in transmission due to ready access to host lungs and mucus membranes without much time for infectivity to decay, while particles that have settled on surfaces must retain sufficient number while awaiting a host. Exposed high-touch surfaces can be a potential threat in public places where there is continuous depositing of infectious virions by passersby.

Although fomite transmission of Influenza and SARS-CoV-2 is uncommon, the fact that infectivity persists for a long time on surfaces make it a very plausible method of transmission. The emergence of new strains of SARS-CoV-2 or pandemic Influenza with a heightened ability to persist on and infect from fomites is a real threat and one that requires further research into the behavior of these viruses outside the body. As a result, there have been several elegant solutions for the production of anit-viral surface coatings to mitigate this threat[24,25]. However, these coatings are not yet commercialized or universally available. Hence it is important to understand the physical conditions that prolong the viability of viruses as they collect on surfaces from drying fomite particles.

To better understand the forces virions, contend with in drying droplets, our group sought to quantify the impact of changing concentrations of solutes on Influenza and SARS-CoV-2 virions. Respiratory droplets contain many solutes, including proteins, mucins, surfactants, and salt[26]. We investigated salt's role specifically, because of its impact on protein folding and the osmotic stress it places on viral membranes.

High concentrations of salt, like those found in drying respiratory droplets, have been used for millennia to preserve food due to its ability to prevent microbial growth[27]. Since viruses are not biologically active outside of host cells, it is important to determine if they can withstand non-physiological conditions and become infectious again when inhaled.

It is possible that there is some component of respiratory droplets that protects virions from the impacts of extreme salt concentrations that occur while drying. Identifying salt's impact in the absence of other solutes will demonstrate if the resilience shown in other studies is intrinsic or extrinsic to respiratory viruses.

The makeup of droplets deposited on surfaces can vary, leading to different conditions experienced by the deposited virions and different evaporation rates. There are notable differences in the levels of solutes present in saliva and upper respiratory secretions, which might be coughed up when ill. While mucin levels in saliva and respiratory secretions are similar in healthy individuals with saliva 1.2 ± 0.2 mg/mL[28] compared to respiratory secretions containing 1.5 ± 0.15 mg/mL[29], during infection levels of mucin significantly increase[30] and accounting for how mucin impacts drying rates and droplet conditions is important factor to consider.

The surfaces that the droplet lands on can similarly impact the drying rate of the droplet due to interactions between the surfactant in the droplets and the substrate upon which the droplets are placed. The surfactants can also form a ring at the air/liquid interface pinning the droplet edge, and preventing contraction. This "frustrated" mode can increase the drying time significantly contributing to the survivial of viruses contained within the droplets[31–33]. In addition, as the water evaporates, the NaCl concentration within the droplet increases, and it becomes important to understand the effect of high saline concentration on the viral proteins and infectivity.

2. Methods

2.1. Droplet Drying Experiments

Droplets of 1–2 µL of 154 mM NaCl or of pig upper respiratory fluid (obtained from post mortem female York-shire pigs (~25kg) sacrificed in non-related IACUC approved research) the approximate size of large respiratory droplets[23], are pipetted onto glass substrate at 297K and 45% relative humidity. Evaporation was measured by changes in volume using contact angle goniometry and changes in mass using a microbalance. Measurements of droplet mass (mg) and NaCl concentration are taken every 1 minute for 50 minutes.

2.2. Plaque assay experiments

To determine the impact of NaCl on virus infection, plaque assays are carried out on attenuated SARS-CoV-2 (Codagenix) incubated for 1 hour in DMEM solution supplemented with NaCl[34]. Serial

dilutions are conducted and the virus is incubated with Vero E6 cells (WHO 10-87) in DMEM with 2% FBS for 1 hour at 37 °C. The virus medium is then removed, and cells were covered (2X MEM: 1.2% Tragacanth (Sigma): MEM) (1:1:2) supplemented with 0.5% TrypLE Select (Gibco) 1% Pen Strep (Gibco). Cells are grown for 4 days at 33 °C and are stained and fixed with 1% crystal violet, 3.7% formaldehyde.

To quantify the plaque-forming units (pfu) of H1N1 virus (ATCC® VR-95™), MDCK2 (NBL-2) (ATCC® CCL-34™) cells were used in a plaque assay. The virus was incubated for 1 hour in MEM Alpha with 0.2% BSA, followed by serial dilutions. The diluted virus was then incubated with MDCK2 cells for 30 minutes at room temperature, and for an additional hour in a 37°C 5% CO_2 incubator. The virus medium was removed, and a semi-solid medium was added, containing a quarter volume of 1.2% Tragacanth, a quarter volume of 2X MEM Alpha, 0.2% BSA, 0.5% TrypLE Select, and half volume of MEM Alpha. The plates were then incubated for 72 hours at 33°C 5% CO_2. After incubation, the plates were rinsed and stained with a solution containing 1% crystal violet, 3.7% formaldehyde, and 50% methanol.

The number of plaques on dilution plates containing 5-50 pfu's were counted, and taking into consideration the inoculum dilution added into counted plates, the number of surviving viruses pfu was reported relative to the control sample as the log-reduction of pfu caused by the salt treatment.

2.3. 3D Molecular Imprinting

Molecular imprinted sensors were fabricated by using an imprinting solution which is a mixed solution of S-protein (IRB 1212002) in Dulbecco's phosphate buffered saline (dPBS) and alkanethiol in DMSO. The electrical resistance of these sensors changes if there is solute bound to them, and allows us to quantitatively measure the binding of our specifically imprinted solute. Then, to prepare the assay solution, the S- protein is diluted in double distilled water or dPBS, and NaCl is added to a target concentration of 0.0 M, 0.15 M, or 5.0 M, at 297K for 1 hour. An open circuit potentiometer (Lawson Laboratories, Model EMF16) was used to analyze the re-adsorption of the treated S-protein on the molecular imprinted surface by monitoring the potential change of the biosensor without applying an external electric field. A 3-electrode system was used; 1 Ag/AgCl electrode as the reference electrode, 1 Ag/AgCl electrode as the common ground electrode, and 1 Au chip imprinted with pristine S-protein was used as the working electrode. The 3 electrodes were all placed in a 10 mL beaker with 8 mL 1X dPBS continuously stirred with a magnetic stirrer and stir bar at 300–500 rpm. A known amount of the assay solution was pipetted dropwise into the detection system in intervals after allowing the system to come to equilibrium while the OCP was recorded in real-time using the L-EMF DAQ software. The detected electrical response signal was normalized as $[\Delta V/V_0] = (V - V_0)/V_0$, where V is the detected real-time potential and V_0 is the initial saturated potential.

2.4. Molecular Dynamics Simulations

AAMD simulations are performed using GROMACS 2020.2 on the AiMOS supercomputer built with IBM POWER9 and NVIDIA Volta V100 GPUs[35,36], and use the initial structure (PDB: 6VXX) [37]. The AMBERsb14 package with Joung and Cheatham (JC) ion parameters is used to parameterize the system[38–40]. We run four simulations at NaCl concentrations of 0.0 M, 0.5 M, 1.0 M, and 1.5 M with

TIP3P water. These concentrations are achieved by replacing water molecules with the appropriate numbers of Na^+ and Cl^- ions. The S-protein, 12×13×16 nm^3, is immersed in a water box of 20×20×20 nm^3 for the first three concentrations while 1.5 M requires a 25×25×25 nm^3 to allow for ion placement. Next, additional Na+ ions are added to neutralize the charge of the overall system. Periodic boundary conditions are applied to all three dimensions. Before production runs with time step size of 2 fs, each simulation undergoes multi step equilibration including energy minimization for 100 ps, NVT for 100 ps to heat the system to 297 K, and NPT equilibration for 100 ps to bring the system to 1 atm. The in-silico experiments are run for 2.5 μs in the 0.0 M, 0.5 M, and 1.0 M simulations while the 1.5 M simulation was run for 2 μs due to the system size. Salt bridges (Supplemental Data) are identified using approximately the last 1,000 frames of each simulation trajectory and the Timeline module of VMD with a cutoff distance of 0.32 nm[41]. We determine the duration of each salt bridge in terms of frame percentage, defined by the fraction of total frames during which two residues meet the salt bridge definitions based on their geometry.

3. Results

Viral particles are typically released into the air within droplets that are expelled from the respiratory system. These droplets commonly contain NaCl and lung surfactant proteins. Depending on their size and weight, the droplets may either remain suspended in the air or settle onto surfaces. The survival of the viruses contained within the droplets is influenced by the internal conditions of the droplets, which are in turn affected by the rate of droplet drying. The drying rate of colloidal particles is known to be influenced by the surfactant that encapsulates them, as well as by the interactions that occur between the surfactants and the solid-liquid interface when the droplets settle onto surfaces[42]. To study this, we compared the drying dynamics of water, physiologic NaCl solution (saline), and pig upper respiratory fluid droplets on glass substrates using a micro-balance. The results are shown in Figure 1, where we can see that in the first 20 minutes, the dynamics of all the droplets obeyed a linear function, where the saline and lung fluid droplets dried at the same rate while water dried approximately 25% faster. The water droplets fully evaporated within 30 minutes, whereas the saline and lung fluid droplets followed a slow asymptotic function, leaving behind 4% and 12% of their original mass after at least 50 minutes, respectively. Notably, this is more than can be accounted for by the mass of solutes, implying that there is water trapped in these dried residues as well.

Drying of liquid droplets has been shown to proceed either by reduction in radius, when the air-liquid-surface interface is free to move, or by reduction in height, when the droplet is pinned at the air-liquid-surface interface. According to Wu et al., the pinning occurs due to accumulation of surfactant, which interacts strongly with both the liquid and the solid phases and leads to the production of broad ring patterns[42]. In Figure 2 we show optical microscopy images of the droplets after drying. In the case of saline (Figure 2A), the rim of the droplet is marked by several salt crystals which can be seen to partially pin the droplet. When other biological substances are added a larger ring is formed that pins the entire rim of the droplet and can retain fluid for longer times. Initially, the saline and lung fluid droplets are assumed to contain similar NaCl concentrations, with lung surfactants being a minor component. In Figure 1 we plot the increase in NaCl concentration within the droplets as the water evaporates, using

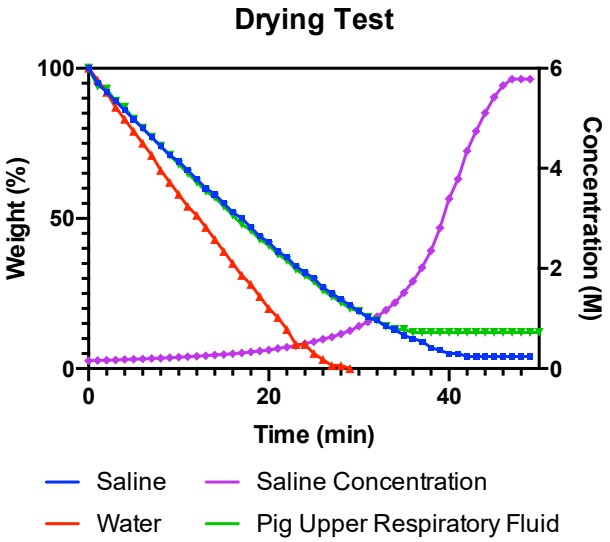

Figure 1. Weight loss rate and NaCl concentration of a 2 µL droplet deposited on a glass slide. The droplet was either 0.15 M saline, DI water or undiluted pig lung fluid.

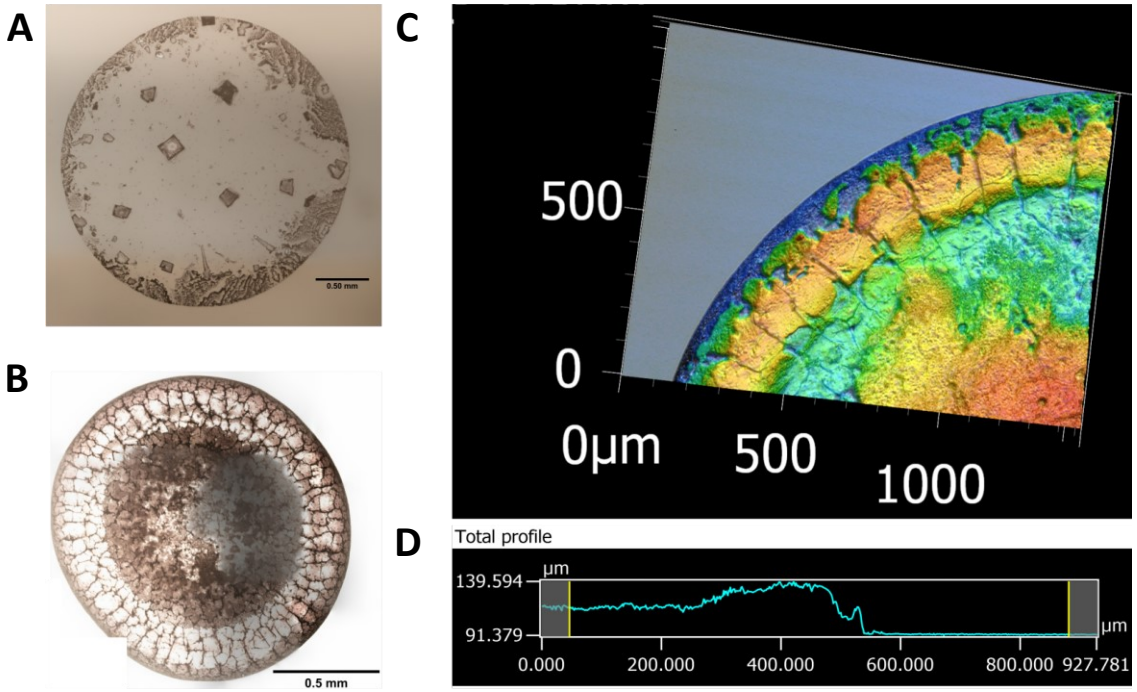

Figure 2. Optical image of 2 µL droplets dried on glass. (A) 0.15 M saline droplet–note dried NaCl cubic crystals (B) Lung fluid droplet: top view and (C) Topographical details (D) Corresponding cross-sectional analysis.

the data from the saline droplets, which we assume to form an upper limit estimate for the lung fluid droplet. If lung fluid droplets were to contain viral particles, it would be crucial to establish whether their infectivity remains intact as the NaCl concentration rises. To investigate this, we conducted an experiment to assess the infectivity of H1N1 and SARS-CoV-2 viral particles after being exposed to NaCl solutions of varying molarities, as shown in the accompanying Figure 3, for a duration of 1 hour.

3.1. Plaque Assays

Plaque assays reflect the aggregate function of components vital to viral infection and replication. Samples containing viruses are added to cell culture plates, and the number of infectious virions in the sample can be measured indirectly by the number of areas of cell death, called plaques, which are quantified as a measure of viral titer. Damage to any part of the virus necessary for infection or replication, the S-protein, genetic material, envelope, or other systems, will prevent viruses from forming plaques.

In Figure 3A we show the plates following viral infection with SARS-CoV-2 particles incubated in NaCl solution of different concentrations for 1 hour. We can immediately see that plaques have formed at all the concentrations studied, ranging from 0.1 to 5.0M. We found no significant differences in the infectivity of attenuated SARS-CoV-2, determined by a two tailed t-test where the lowest p-value was between 0.11 M and 1.0 M at 0.27. The log reductions obtained from these plates are plotted in Figure 3B, where we can see that in all cases no larger than 0.1 log reduction has occurred regardless of salt concentration. A similar experiment was also conducted for H1N1 influenza virus and is plotted in Figure 3B as well, where we can see that the maximum log reduction that occurred was no larger than 0.8. Hence NaCl appears to have a minimal effect on infectivity of both types of enveloped viruses.

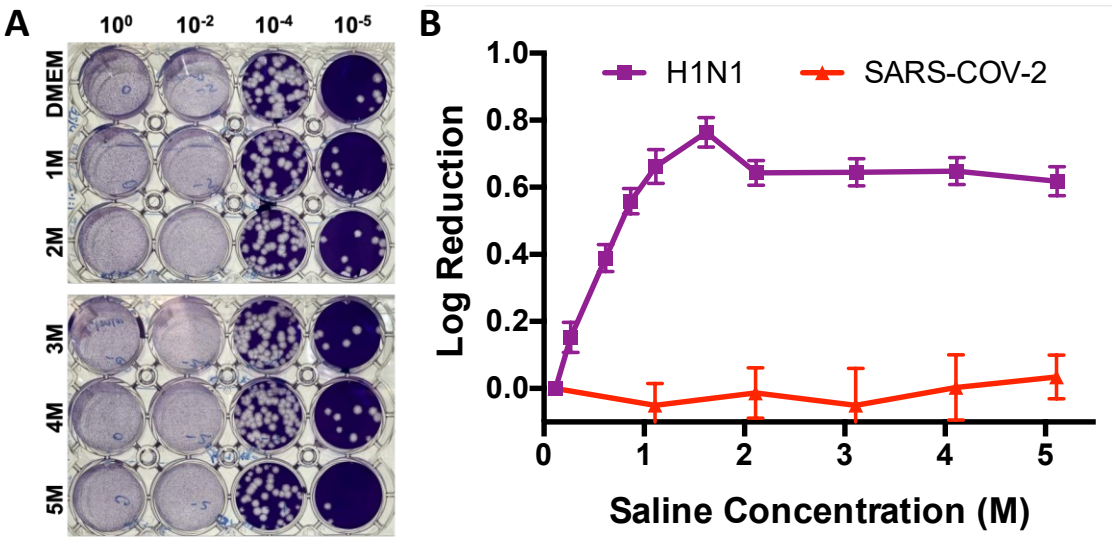

Figure 3. (A) Optical images of the plaque assay plate for SARS-CoV-2 viruses exposed for 1 hour to NaCl solutions of different concentrations. DMEM is the control, containing 0.11 M of NaCl. Plaques are clearly visible at all concentrations. (B) Log reduction plotted as a function of NaCl concentration for H1N1 virus and SARS-CoV-2.

3.2. 3D molecular imprinting

SARS-CoV-2 uses the Spike (S) protein to bind to angiotensin-converting enzyme 2 (ACE2) and infect host cells[20]. Maintaining the structural integrity of the S-protein is therefore essential in preserving the infectivity of the virus. Previously, we have used molecular imprinting to detect influenza viral particles and S-proteins[43]. This technique, which uses 3D templating in combination with surface topographical features to detect analytes ranging from a few nm to several hundred nm, was shown to

discriminate between H1N1 and H3N2 particles and between S-proteins from SARS-CoV-2 and MERS viral particles. This technique was also able to detect small changes in the H1N1 and the S-protein conformation with increasing temperature, which correlated with the corresponding decrease in viral infectivity[43]. The sensitivity of this technique to small changes in protein structure was further demonstrated using sensors imprinted for hemoglobin (Hg), which were able to detect the subtle changes to the structure of Hg.

To investigate the potential conformational changes of the S-protein in response to varying NaCl concentrations, we conducted experiments on soluble S-protein to determine if there were small changes that did not impact infectivity. We utilized open circuit potential (OCP) response curves, which quantify the binding of analytes to a chip imprinted with the soluble Wuhan strain S-protein from the Center for Systems and Synthetic Biology, University of Texas, Austin. In Figure 4, we present the results, which demonstrate that there are no significant changes in the response after exposing the S-protein analytes to NaCl solutions with concentrations of 0.0 M, 0.15 M, and 5.0 M for 1 hour. These findings are consistent with the retention of infectivity observed in the plaque assay.

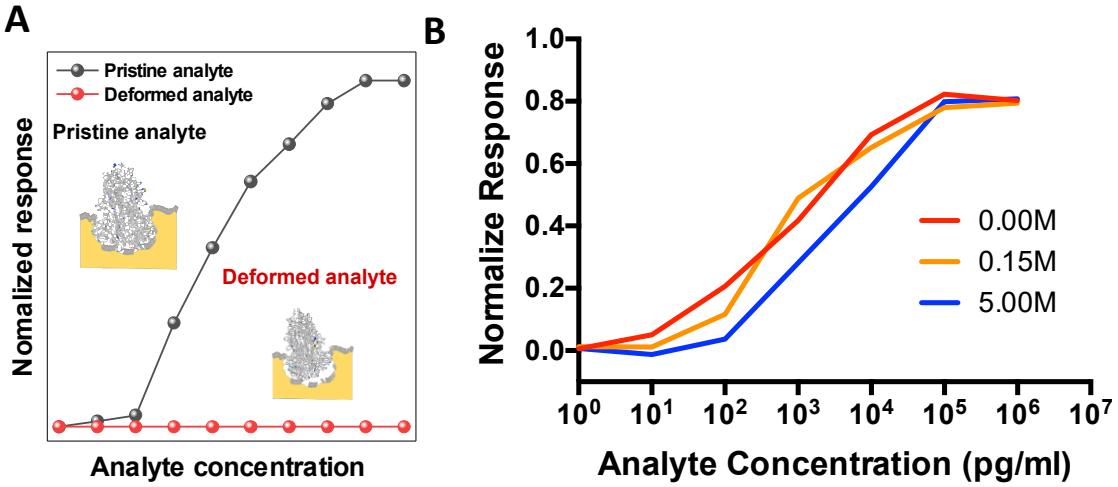

Figure 4. (A) Schematic diagram illustrating expected results for denatured analyte (B) Normalized potentiometric response as a function of analyte concentration for an electrode molecularly imprinted for the SARS-CoV-2 spike protein, where the analyte consisted of spike proteins exposed to 0, 0.15 and 5.00 M NaCl for 1 hour.

3.3. In Silico simulation

Experimentation with SARS-CoV-2 and other highly infectious viruses can be difficult, since it requires BSL-3 enclosures, while computational modeling and simulation experiments can yield answers in a timely manner in order to maintain relevance. Computationally modeling the behavior of the structure of the entire SARS-CoV-2 viral particle in increased NaCl conditions would be extremely time and resource intensive. The S-protein, on the other hand, is more feasible to model and analyze using computational approaches. Since this membrane protein is responsible for initiating the infection cascade, we were prompted to determine whether NaCl was responsible for any significant structural changes. We then compared in silico results with the findings of laboratory bench experiments. In this manner, we validate molecular dynamics simulations of the S-protein run on the AiMOS supercomputer, a

heterogeneous system of IBM POWER9 CPUs and Nvidia V100 GPUs, to predict the infectivity of viral particles under different conditions.

In silico experimentation is widely useful in quantifying subtle and large fluctuations in protein conformation under different environmental conditions. In this present work, we perform a long-term simulation of the S-protein along with a variety of calculations to examine aspects of protein structure spanning both macro and micro levels. Such an approach has the power to predict the response of the S-protein to varied environments as well as the outcomes of in vitro experiments. It also allows for the measurement of the S-Protein in-situ while exposed to salt. Our in vitro studies exposed the S-protein to high levels of salt then measured for any lasting changes in more physiological conditions. In silico modeling allows us to capture even small and transient fluctuations in the S-Protein's structure that might help to elucidate the relationship that it has with high salt concentrations.

The NaCl concentrations of in silico experiments were selected based on the results of droplet drying experiments (highlighted in Figure. 1). The largest droplet with a size of 2 µL took 30 minutes to reach a NaCl concentration of 1.0 M and approximately 45 minutes to reach 5.0–6.0 M. With these measurements we parameterize the in silico model by selecting concentrations of 0.0 M, 0.5 M, 1.0 M, and 1.5 M, 1.5 M was the maximum achievable concentration using GROMACS 2020.2 software.

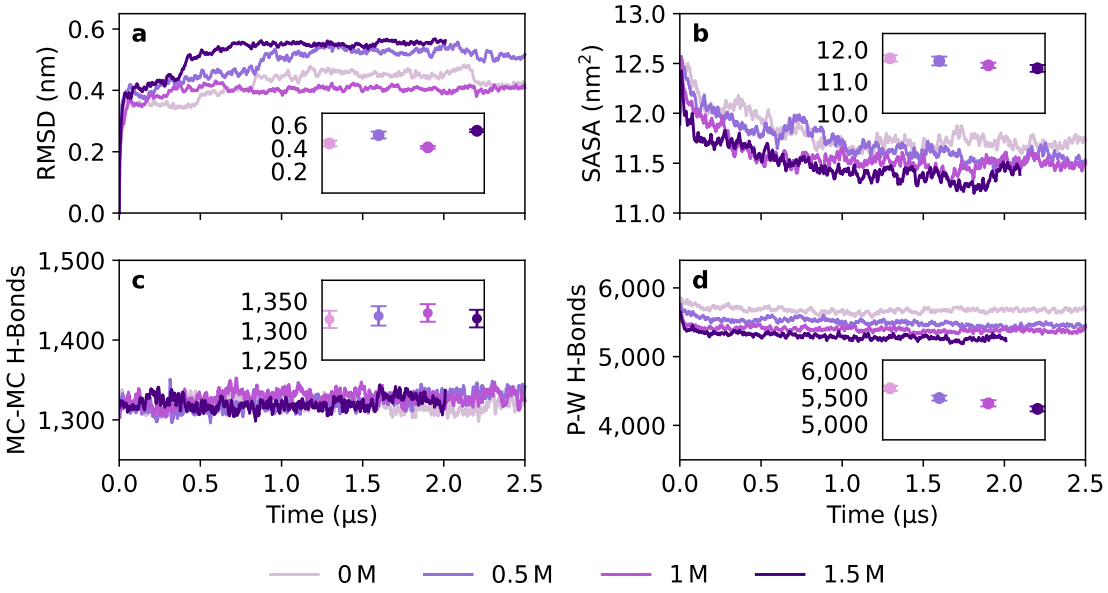

Figure 5. Full time series and µ ± δ of structural measurements. Increasing NaCl concentrations are indicated by increasing depths of purple. The (A) RMSD and (B) SASA measurements relative to the initial frame in time series. We highlight the narrow distribution of RMSD means and SASA means in A and B, respectively. The numbers of (C) P-W and (D) MC-MC H-Bonds relative to the initial frame in time series. We highlight the narrow distribution of MC-MC H-bond means and P-W H-bond means in C and D, respectively.

Time series measurements of RMSD, SASA, MC-MC H-Bonds, and P-W H-Bonds do not reflect any significant changes in S-protein conformation using the initial structure as reference, as there are no irregular increases in any of the curves across all four measurements (Figure 5). These data sets are

analyzed in terms of statistical significance with corresponding $\mu \pm \delta$ also shown in Figure 5, showing the relatively constant means of each of these measurements after 500 ns.

The RMSD of the S-protein backbone describes the amount by which the backbone structure has deviated from its starting position, and it is used to analyze whether the system has reached equilibrium. The RMSD time series curves remain relatively constant after 500 ns, showing that each of the four MD systems equilibrate. The SASA of the entire S-protein also remains relatively unchanged across increasing concentration simulation. Simulations overall show that: (1) Each MD system reaches equilibrium and RMSD minimally changes between 0.0 M and 1.5 M (difference of 0.11 nm); (2) SASA changes $\leq$ 0.31 nm^2 and decreases by an insubstantial 2.7% indicating no large changes between simulations; (3) MC-MC H-bonds differ by $\leq$ 0.08% and μ of all experiments are within one δ show no substantive changes ; (4) P-W H-bonds have a percent decrease between 0.0 M and 1.5 M of 7% again showing no substantive changes; and (5) Mean RMSF changes by < 0.02 nm with low DJS between estimated probability densities indicating that residue flexibility does not differ much among our tested conditions, showing that increased NaCl concentration does not significantly impact S-protein structure.

4. Conclusion

Our combined plaque assay and 3D molecular imprinting experiments led to a significant discovery: varying NaCl concentrations in drying saline droplets do not have a significant impact on viral infectivity or S-protein conformation. In addition, our computational modeling results aligned with the outcomes of the plaque assays and 3D molecular imprinting experiments while also confirming that no reversible changes occur via our in silico results. Our in silico analysis indicates that the S-protein can maintain its structural stability at high NaCl concentrations of 1.5 M, or about ten times the physiological concentration in humans, and even as high as 5 M, which is the concentration that persists for at least one hour in a two-microliter droplet on a glass surface. Our findings have important implications, potentially shedding light on why SARS-CoV-2 is highly transmissible and can survive on surfaces for an extended period of time. Furthermore, this work advances our knowledge on preventative measures and preservation techniques for S-protein samples in laboratory settings.

Acknowledgments

The project is sponsored by OVPR&IEDM COVID-19 Seed Grant (PI: P.Z.) and the Morin Charitable Trust (PI: M.R.), SUNY-IBM Consortium Award (PI: Y.D.) and an IBM Faculty Award FP0002468 (PI: Y.D.) through which we accessed the AiMOS supercomputer at Rensselaer Polytechnic Institute and the WSC Cluster at the IBM Thomas J Watson Research Center to carry out all in silico experiments reported here. We acknowledge and thank Garcia scholars Anand Srinivasan and Junsang Yoon for their work on this project.

Conflicts of Interests

The authors declare no conflict of interest.

Authors' Contribution

Conceptualization, K-C.F., J.F.M., K.S., M.S., K.L., Y.D., P.Z. and M.R.; investigation, K-C.F., F.Y., W-I.L. and S.M.; molecular dynamics simulations data curation, K.S., J.F.M., A.K., K.H., K.L., P.Z. and Y.D.; writing—original draft preparation, K-C.F., J.F.M., K.S. and W.-IL.; writing—review and editing, K-C.F., J.F.M., K.S. and M.R.; funding acquisition, P.Z., Y.D., and M.R.; supervision, P.Z., Y.D., M.K.

Supplemental Data

To further analyze the S-protein structure we identify a number of salt bridges, important in protein stability, that remain intact between the 0.0 M and 1.5 M simulations[44]. These are displayed in Table S1 and Figure S1, and reveal more specific regions where there are no substantial structural changes under increased NaCl concentration.

Table S1. Table Caption Salt bridges common between 0.0 M and 1.5 M identified using the VMD Timeline module that are intact in at least 85% of approximately the last 1,000 frames of each simulation.

Title 1	Amino Acids (Residue. Chain)
Chain A	GLU191.A-ARG34.A, ASP228.A-LYS41.A, ASP53.A-LYS195.A, ASP442.A-ARG509.A, ASP290.A- ARG273.A, ASP663.A-LYS310.A, ASP398-ARG355.A, GLU773.A-ARG1019.A, GLU725.A-LYS1028.A, ASP40.A-ARG44.A, ASP578.A-ARG328.A
Chain B	ASP40.B-ARG44.B, ASP663.B-LYS310.B, GLU1031.B-ARG1039.B, ASP775.B-LYS733.B, GLU406.B-ARG403.B, ASP442.B-ARG509.B, ASP53.B-LYS195.B, GLU819.B-ARG815.B, GLU725.B-LYS1028.B, ASP398.B-ARG355.B, ASP290.B-ARG273.B, ASP578.B-ARG328.B, GLU191.B-ARG34.B
Chain C	ASP775.C-LYS733.C, ASP578.C-ARG328.C, GLU725.C-LYS1028.C, GLU1031.C-ARG1039.C, GLU191.C-ARG34.C, ASP290.C-ARG273.C, ASP40.C-ARG44.C, ASP53.C-LYS195.C
Inter-chain	ASP1118.A-ARG1091.C, ASP994.A-ARG995.C, GLU406.C-ARG408.A, ASP994.B-ARG995.A, GLU1031.B-ARG1039.A, GLU1017.A-ARG1019.B, GLU868.C-ARG646.B, GLU1031.C-ARG1039.B, GLU1017.B-ARG1019.C

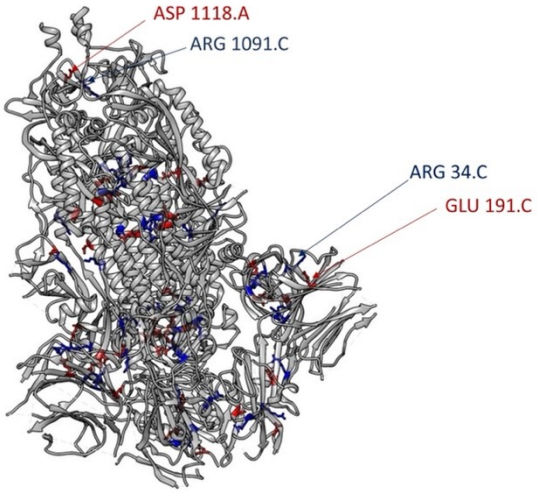

Figure S1. Salt bridges identified in 0.0 M and 1.5 M in silico experiments that are intact in at least 85% of approximately the last 1,000 frames of each simulation. Positive residues are colored blue while negative residues are colored red. This image was created using UCSF Chimera 1.15rc.

References

[1] Dong E, Du H, Gardner L. An interactive web-based dashboard to track COVID-19 in real time. *Lancet Infect Dis*. 2020, 20(5):533–4.

[2] Meyerowitz EA, Richterman A, Gandhi RT, Sax PE. Transmission of SARS-CoV-2: A Review of Viral, Host, and Environmental Factors. *Ann Intern Med.* 2021, 174(1):69–79.

[3] Onakpoya IJ, Heneghan CJ, Spencer EA, Brassey J, Plüddemann A, Evans DH, et al. SARS-CoV-2 and the role of fomite transmission: a systematic review. *F1000Res.* 2021, 24;10:233.

[4] Pitol AK, Julian TR. Community Transmission of SARS-CoV-2 by Surfaces: Risks and Risk Reduction Strategies. *Environ Sci Technol Lett.* 2021, 8(3):263–9.

[5] Charlotte N. High Rate of SARS-CoV-2 Transmission Due to Choir Practice in France at the Beginning of the COVID-19 Pandemic. *J Voice.* 2023, 37(2):292.e9-292.e14.

[6] Koizumi N, Siddique AB, Andalibi A. Assessment of SARS-CoV-2 transmission among attendees of live concert events in Japan using contact-tracing data. J Travel Med [Internet]. 2020, 27(5). Available from: http://dx.doi.org/10.1093/jtm/taaa096

[7] Herstein JJ, Degarege A, Stover D, Austin C, Schwedhelm MM, Lawler JV, et al. Characteristics of SARS-CoV-2 Transmission among Meat Processing Workers in Nebraska, USA, and Effectiveness of Risk Mitigation Measures. *Emerg Infect Dis.* 2021, 27(4):1032–8.

[8] Xie C, Zhao H, Li K, Zhang Z, Lu X, Peng H, et al. The evidence of indirect transmission of SARS-CoV-2 reported in Guangzhou, China. *BMC Public Health.* 2020, 20(1):1202.

[9] van Doremalen N, Bushmaker T, Morris DH, Holbrook MG, Gamble A, Williamson BN, et al. Aerosol and Surface Stability of SARS-CoV-2 as Compared with SARS-CoV-1. *N Engl J Med.* 2020, 382(16):1564–7.

[10] Riddell S, Goldie S, Hill A, Eagles D, Drew TW. The effect of temperature on persistence of SARS-CoV-2 on common surfaces. *Virol J.* 2020, 17(1):145.

[11] Chia PY, Coleman KK, Tan YK, Ong SWX, Gum M, Lau SK, et al. Detection of air and surface contamination by SARS-CoV-2 in hospital rooms of infected patients. *Nat Commun.* 2020, 11(1):2800.

[12] Aboubakr HA, Sharafeldin TA, Goyal SM. Stability of SARS-CoV-2 and other coronaviruses in the environment and on common touch surfaces and the influence of climatic conditions: A review. *Transbound Emerg Dis.* 2021, 68(2):296–312.

[13] Paget J, Spreeuwenberg P, Charu V, Taylor RJ, Iuliano AD, Bresee J, et al. Global mortality associated with seasonal influenza epidemics: New burden estimates and predictors from the GLaMOR Project. *J Glob Health* 2019, 9(2):020421.

[14] Richard M, Fouchier RAM. Influenza A virus transmission via respiratory aerosols or droplets as it relates to pandemic potential. *FEMS Microbiol Rev.* 2016, 40(1):68–85.

[15] Asadi S, Gaaloul Ben Hnia N, Barre RS, Wexler AS, Ristenpart WD, Bouvier NM. Influenza A virus is transmissible via aerosolized fomites. *Nat Commun.* 2020, 11(1):4062.

[16] Thomas Y, Vogel G, Wunderli W, Suter P, Witschi M, Koch D, et al. Survival of influenza virus on banknotes. *Appl Environ Microbiol.* 2008, 74(10):3002–7.

[17] Greatorex JS, Digard P, Curran MD, Moynihan R, Wensley H, Wreghitt T, et al. Survival of influenza A(H1N1) on materials found in households: implications for infection control. *PLoS One* 2011, 6(11):e27932.

[18] Yang W, Elankumaran S, Marr LC. Relationship between humidity and influenza A viability in droplets and implications for influenza's seasonality. *PLoS One* 2012, 7(10):e46789.

[19] Kraay ANM, Hayashi MAL, Hernandez-Ceron N, Spicknall IH, Eisenberg MC, Meza R, et al. Fomite-mediated transmission as a sufficient pathway: a comparative analysis across three viral pathogens. *BMC Infect Dis.* 2018, 18(1):540.

[20] Morens DM, Rash VM. Lessons from a nursing home outbreak of influenza A. Infect Control Hosp Epidemiol. 1995, 16(5):275–80.

[21] Zhou L, Ayeh SK, Chidambaram V, Karakousis PC. Modes of transmission of SARS-CoV-2 and evidence for preventive behavioral interventions. *BMC Infect Dis.* 2021, 21(1):496.

[22] Jayaweera M, Perera H, Gunawardana B, Manatunge J. Transmission of COVID-19 virus by droplets and aerosols: A critical review on the unresolved dichotomy. *Environ Res.* 2020, 188:109819.

[23] Duguid JP. The size and the duration of air-carriage of respiratory droplets and droplet-nuclei. *J Hyg* 1946, 44(6):471–9.

[24] Bobrin VA, Chen S-P, Grandes Reyes CF, Sun B, Ng CK, Kim Y, et al. Water-Borne Nanocoating for Rapid Inactivation of SARS-CoV-2 and Other Viruses. *ACS Nano* 2021, 15(9):14915–27.

[25] Bobrin VA, Chen S-PR, Grandes Reyes CF, Smith T, Purcell DFJ, Armstrong J, et al. Surface Inactivation of Highly Mutated SARS-CoV-2 Variants of Concern: Alpha, Delta, and Omicron. *Biomacromolecules* 2022, 23(9):3960–7.

[26] Vejerano EP, Marr LC. Physico-chemical characteristics of evaporating respiratory fluid droplets. *J R Soc Interface* [Internet]. 2018, 15(139). Available from: http://dx.doi.org/10.1098/rsif.2017.0939

[27] Doyle ME, Glass KA. Sodium Reduction and Its Effect on Food Safety, Food Quality, and Human Health. *Compr Rev Food Sci Food Saf*. 2010, 9(1):44–56.

[28] Kejriwal S, Bhandary R, Thomas B, Kumari S. Estimation of levels of salivary mucin, amylase and total protein in gingivitis and chronic periodontitis patients. *J Clin Diagn Res* 2014, 8(10):ZC56-60.

[29] Kesimer M, Ford AA, Ceppe A, Radicioni G, Cao R, Davis CW, et al. Airway Mucin Concentration as a Marker of Chronic Bronchitis. *N Engl J Med* 2017, 377(10):911–22.

[30] Li Y, Tang XX. Abnormal Airway Mucus Secretion Induced by Virus Infection. *Front Immunol* 2021, 12:701443.

[31] Tarafdar S, Tarasevich YY, Dutta Choudhury M, Dutta T, Zang D. Droplet Drying Patterns on Solid Substrates: From Hydrophilic to Superhydrophobic Contact to Levitating Drops. *Advances in Condensed Matter Physics* [Internet]. 2018. Available from: https://www.hindawi.com/journals/acmp/2018/5214924/

[32] Bhardwaj R, Agrawal A. Likelihood of survival of coronavirus in a respiratory droplet deposited on a solid surface. *Phys Fluids* 2020, 32(6):061704.

[33] Devineau S, Anyfantakis M, Marichal L, Kiger L, Morel M, Rudiuk S, et al. Protein Adsorption and Reorganization on Nanoparticles Probed by the Coffee-Ring Effect: Application to Single Point Mutation Detection. *J Am Chem Soc.* 2016, 138(36):11623–32.

[34] Wang Y, Yang C, Song Y, Coleman JR, Stawowczyk M, Tafrova J, et al. Scalable live-attenuated SARS-CoV-2 vaccine candidate demonstrates preclinical safety and efficacy. *Proc Natl Acad Sci U S A* [Internet]. 2021, 118(29). Available from: http://dx.doi.org/10.1073/pnas.2102775118

[35] Abraham MJ, Murtola T, Schulz R, Páll S, Smith JC, Hess B, et al. GROMACS: High performance molecular simulations through multi-level parallelism from laptops to supercomputers. *SoftwareX*. 2015 Sep 1;1–2:19–25.

[36] Hanson WA. The CORAL supercomputer systems. *IBM J Res Dev.* 2020, 64(3/4):1:1-1:10.

[37] Walls AC, Park Y-J, Tortorici MA, Wall A, McGuire AT, Veesler D. Structure, Function, and Antigenicity of the SARS-CoV-2 Spike Glycoprotein. *Cell* 2020, 181(2):281-292.e6.

[38] Maier JA, Martinez C, Kasavajhala K, Wickstrom L, Hauser KE, Simmerling C. ff14SB: Improving the Accuracy of Protein Side Chain and Backbone Parameters from ff99SB. *J Chem Theory Comput.* 2015, 11(8):3696–713.

[39] Zgarbová M, Otyepka M, Sponer J, Mládek A, Banáš P, Cheatham TE 3rd, et al. Refinement of the Cornell et al. Nucleic Acids Force Field Based on Reference Quantum Chemical Calculations of Glycosidic Torsion Profiles. *J Chem Theory Comput.* 2011, 7(9):2886–902.

[40] Joung IS, Cheatham TE 3rd. Molecular dynamics simulations of the dynamic and energetic properties of alkali and halide ions using water-model-specific ion parameters. *J Phys Chem B* 2009, 113(40):13279–90.

[41] Humphrey W, Dalke A, Schulten K. VMD: visual molecular dynamics. *J Mol Graph*. 1996, 14(1):33–8, 27–8.

[42] Wu M, Di Y, Man X, Doi M. Drying Droplets with Soluble Surfactants. *Langmuir* 2019, 35(45):14734–41.

[43] Lee W-I, Subramanian A, Mueller S, Levon K, Nam C-Y, Rafailovich MH. Potentiometric Biosensors Based on Molecular-Imprinted Self-Assembled Monolayer Films for Rapid Detection of Influenza A Virus and SARS-CoV-2 Spike Protein. *ACS Appl Nano Mater*. 2022, 5(4):5045–55.

[44] Bosshard HR, Marti DN, Jelesarov I. Protein stabilization by salt bridges: concepts, experimental approaches and clarification of some misunderstandings. *J Mol Recognit.* 2004, 17(1):1–16.